J Mater Sci (2008) 43:4257–4263
DOI 10.1007/s10853-008-2616-z

The effect of annealing on the deformation behaviour and microstructure of crystallized Mg–23.5Ni (wt.%) alloy

M. Eddahbi · P. Pérez

Received: 29 January 2008 / Accepted: 25 March 2008 / Published online: 9 April 2008

Abstract Rapidly solidified amorphous Mg–23.5Ni (wt.%) ribbons were crystallized at 300 and 400 °C for 90 min. After annealing at 300 °C the microstructure was heterogeneous, consisting of rounded eutectic–lamellar domains, which contained magnesium grains smaller than 500 nm. In the case of ribbons annealed at 400 °C the microstructure, however, was homogenous, and composed of well-formed magnesium grains and Mg_2Ni particles. At room temperature both crystallized materials were brittle due to the high volume fraction of Mg_2Ni particles, but they exhibited some ductility with increasing test temperature. Above 200 °C, the microstructure of the ribbons annealed at 300 °C was characterised by the formation of particle free zones during the tensile test. This structure was not observed in the material annealed at 400 °C. Deformation behaviour and changes in the microstructure during plastic flow of both crystallized materials were explained according to grain boundary sliding mechanisms.

Introduction

During the last decades various processing techniques have been developed to produce new ultra-fine-grained magnesium (Mg) alloys as potential candidates for numerous structural applications. At low temperatures, ultra-fine-grained microstructures improve significantly ductility and yield strength, although high strength is sometimes accompanied by low ductility. Furthermore, fine-grained alloys could exhibit superplasticity [1]. Tensile strength in Mg–Ni systems has been reported to be three times higher than that observed in wrought commercial materials [2–4]. Consequently, alloys belonging to the Mg–Ni system seem to constitute an alternative for the processing of high strength magnesium alloys [5, 6].

Numerous studies on different materials and metal systems in a wide range of temperatures and applied stresses have increased significantly comprehension of the mechanisms responsible for microstructural evolution during plastic flow [7–11]. It is well-established that a deformation mechanism is essentially characterized by the stress exponent (n) and the activation energy (Q), which depend on temperature and applied stress or imposed strain rate [12]. For example, stress exponents of 5 and 3 are usually associated with dislocation climb and viscous-glide mechanism, respectively [13]. On the other hand, grain boundary sliding, $n = 2$, is frequently reported as the mechanism controlling the deformation in fine-grained materials [14, 15].

Among the raw materials used for the development of fine-grained materials could be listed atomized or mechanically alloyed powders and melt spun ribbons. The structure in these materials could be amorphous, quasicrystalline and/or nanocrystalline. An attractive alternative route for the production of nanosized materials is crystallization from the amorphous state. Thin shapes such as ribbons, foils or powders can be used as precursors for developing bulk nanocrystalline or nanocomposite materials through the proper consolidation process [16, 17]. In addition, the crystallized microstructure can be optimized through an adequate selection of thermal treatments [18, 19].

M. Eddahbi (✉)
Departamento de Física, Universidad Carlos III, Leganes 28911, Madrid, Spain
e-mail: eddahbi17@yahoo.com

P. Pérez
Centro Nacional de Investigaciones Metalúrgicas (CSIC), Avda. Gregorio del Amo 8, 28020 Madrid, Spain

The present work is part of a global study which involves processing of bulk nanocrystalline Mg–23.5Ni alloy with high mechanical properties. Previous studies on the amorphous Mg–23.5Ni alloy have shown that crystallization occurred through two consecutive stages [20]. In the first stage Mg and metastable $Mg_{5.5}Ni$ were developed. In the second stage, the $Mg_{5.5}Ni$ phase decomposed into Mg and Mg_2Ni particles. With further heating the microstructure evolved towards the eutectic-like structure [21]. The aim of the present study was to show the influence of the initial microstructure on the mechanical properties and deformation mechanisms in rapidly solidified Mg–23.5Ni alloy. Different crystallized microstructures were obtained from the amorphous state through thermal annealing at 300 and 400 °C. Deformation mechanisms were proposed to describe the mechanical behaviour and microstructural changes during tensile tests at temperatures above 200 °C.

Experimental part

Amorphous Mg–23.5Ni (wt.%) ribbons, 39 μm thick and 0.7 mm width, were obtained using the melt-spinning technique. A cylindrical quartz tube, completely flat bottom, with a rectangular orifice of about 4 mm was used as crucible. After inductive heating, the molten alloy was ejected on a cylindrical copper wheel of 20 cm in diameter, using helium gas. The tangential velocity was kept constant at 50 m/s. Distance from the crucible to wheel was between 1 and 0.5 mm. Description of this technique as well as calorimetric measurements carried out in the amorphous ribbons were discussed elsewhere [20].

The mechanical behaviour was studied using a microtensile machine equipped with a load cell of 200 N, a sensitivity of 0.1 N and flat grips. A heating system attached to both grips allowed testing up to 500 °C. Length of the samples was 10 mm. Mechanical tests were conducted in vacuum, between room temperature and 300 °C at an initial strain rate of 10^{-4} s^{-1}. Strain rate change tests were also conducted to determine the apparent stress exponent and activation energy of the deformation mechanism.

Annealing treatments at 300 and 400 °C for 90 min were performed in the tensile machine, prior to tensile tests. The microstructures of annealed and tensile tested samples were examined by field emission gun scanning electron microscope.

Results

Figure 1a and b shows the microstructures of the alloy after annealing at 300 and 400 °C for 90 min, respectively.

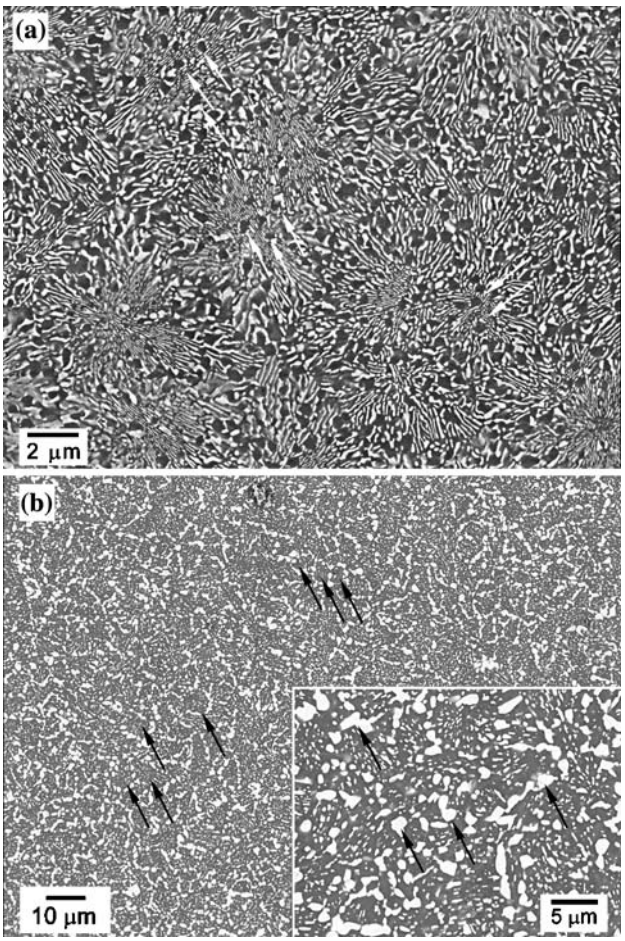

Fig. 1 Microstructures of amorphous ribbon after annealing for 90 min at: (**a**) 300 °C, the arrows indicate the isolated Mg grains and (**b**) 400 °C, the arrows indicate the equiaxed Mg grains. The inset micrograph is a detail showing the coexistence of small coarse Mg_2Ni particles, homogenously distributed in the Mg matrix

Quite clearly, both crystallized microstructures are dissimilar. This is due to differences in phase transformations controlling the crystallization behaviour of amorphous Mg–23.5Ni ribbons, as has been reported previously by calorimetric measurements and microscopic observations in Refs. [20, 21].

The ribbons annealed at 300 °C show a lamellar structure consisting of alternating arrangements of Mg and Mg_2Ni phases, embedding isolated Mg grains up to 500 nm in size. Since the lamellar structure grows in a radial form, the microstructure appears as nearly spherical domains of about 12.5 μm in size. Small Mg grains are mainly located at the borders of the lamellar domains, as shown in Fig. 1a. Nevertheless, in the case of ribbons annealed at 400 °C, the domain structure is not observed. Equiaxed Mg grains, less than 9 μm in size, outlined by coarse Mg_2Ni particles, up to 2 μm in size, are developed instead (see the inset in Fig. 1b). Small Mg_2Ni particles, with whisker and/or plate

morphology, are also found inside Mg grains. Apparently, these particles correspond to those originally constituting the eutectic structure, which undergo further growth in their thickness direction.

Figure 2 shows the true stress–true strain curves for both annealed materials deformed in tension at temperatures up to 300 °C at an initial strain rate of 10^{-4} s^{-1}. The material annealed at 300 °C is brittle below 100 °C, as shown in Fig. 2a. Between 100 and 150 °C, ribbons exhibit high strength but fracture takes place immediately after the yield stress is surpassed. Above 150 °C, once the ultimate tensile stress is attained, the stress decreases with the strain until failure and the elongation to failure increases up to 16% at 300 °C.

In the case of material annealed at 400 °C, the ribbon failure occurs in the elastic regime at room temperature, but the material exhibits some ductility above 50 °C (see Fig. 2b). At 50 °C, the material seems to support a high stress level of about 250 MPa, but the failure takes place immediately after the yield stress. At 100 °C, the elongation increases up to 1.5%, although the strength reaches 230 MPa. At higher temperatures, a sharp decrease in the yield stress, accompanied by a substantial elongation increase, is noticed. At temperatures up to 200 °C, the alloy annealed at 300 °C exhibits higher strength than the material annealed at 400 °C, being the opposite true at test temperatures above 200 °C.

Since both materials are brittle at room temperature, the strength has been estimated through the microhardness Vickers measurements (HV), applying the relationship $\sigma_y = 9.8HV/3$, where σ_y is the yield stress [22, 23]. Introducing hardness values of 170 and 123HV in this equation, the yield stress values are of about 550 and 402 MPa for the material annealed at 300 and 400 °C, respectively. Fine arrangements of Mg and Mg_2Ni lamellae in the eutectic-like domains provide high strength up to temperatures of about 150 °C for the material annealed at 300 °C. The lower microhardness of the alloy annealed at 400 °C should be related to Mg_2Ni coarsening.

Figure 3 plots the true strain rate–true stress in double logarithmic scale for both annealed materials at test temperatures from 200 to 300 °C. The stress values were obtained from the true stress–true strain curves of Fig. 2 for a fixed strain of 2%. Data in Fig. 3 were fitted to a power law constitutive creep equation given below [24, 25]

$$\dot{\varepsilon} = k\sigma^{n_a} e^{(-Q_a/RT)},$$

where k is the creep constant, n_a the apparent stress exponent which is the slope of curves in Fig. 3, σ the stress in the steady state, Q_a the apparent activation energy of the deformation mechanism, T the absolute temperature and R the universal gas constant. At all test temperatures the data

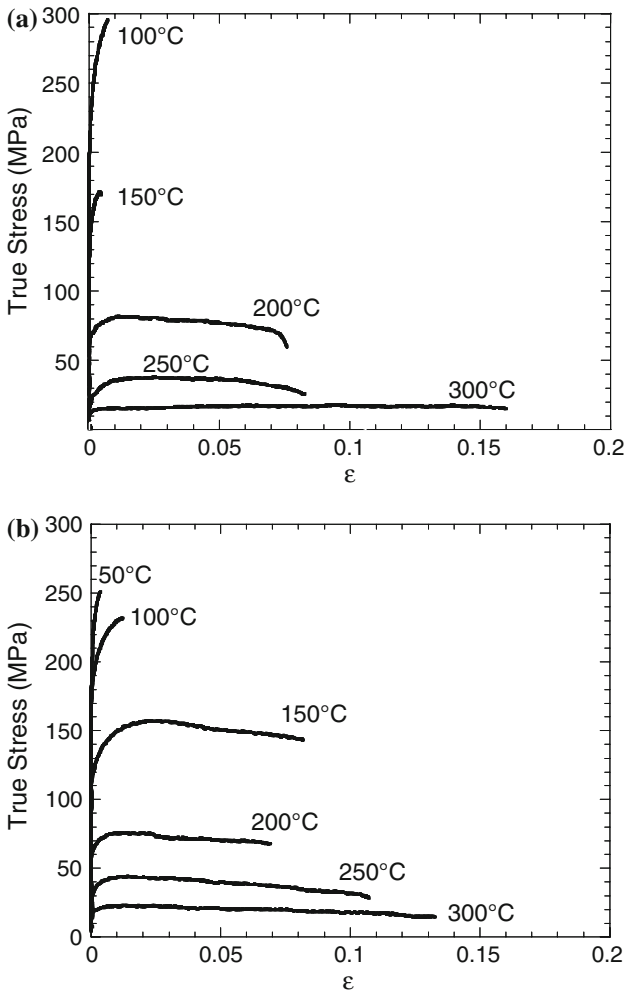

Fig. 2 True stress–true strain curves at different temperatures at 10^{-4} s^{-1} corresponding to: (**a**) annealed material at 300 °C/90 min and (**b**) annealed at 400 °C/90 min

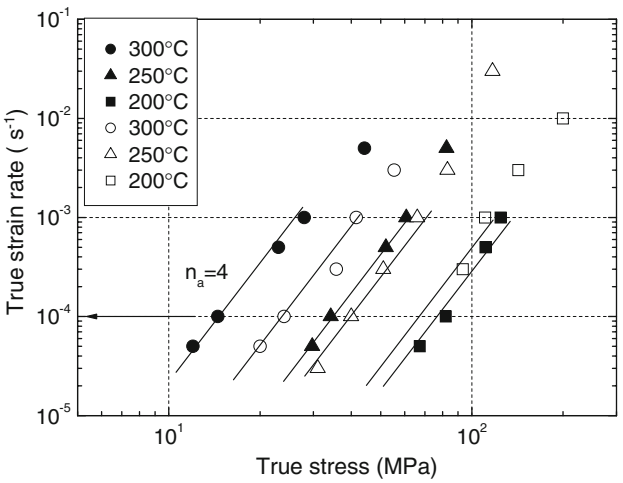

Fig. 3 True strain rate–true stress at different temperatures of annealed materials. The open and solid symbols correspond to the material annealed at 300 and 400 °C, respectively

in the vicinity of 10^{-4} s^{-1} can be fitted to a power law, with a slope of $n_a = 4$, as illustrated in Fig. 3. The activation energy of the deformation process was determined plotting the true stress corresponding to the strain rate of 10^{-4} s^{-1} as a function of the inverse of the temperature. Values of 93 and 115 kJ/mol were calculated for the materials annealed at 300 and 400 °C, respectively. It is apparent that these activation energies are between the activation energy corresponding to the Mg lattice self-diffusion, and that associated with the grain boundary diffusion, 135 and 92 kJ/mol, respectively [26].

Several microstructural observations were carried out in the ribbons tensile tested at different temperatures. For the material annealed at 300 °C, the microstructures of deformed samples to strain of 8 and 16% at 250 and 300 °C are shown in Fig. 4a and b, respectively. These micrographs are quite different from that of crystallized ribbons, displayed in Fig. 1. Particle free zones (PFZs) are developed normal to the tensile axis, outlining the original domains [27]. It was observed that the higher the temperature the thicker the PFZs, see Fig. 4. In the case of ribbon annealed at 400 °C, the microstructure of deformed samples apparently resembles that of the non-deformed material, as shown in Fig. 5 for a sample tested at 300 °C. It is worth noting that PFZ acronym refers only to the singular structure observed at domain boundaries, seen in Fig. 1, but it is not related to the development of precipitates free zones or denuded zones reported for some magnesium and aluminium alloys. In these materials, the deformation mechanism as well as the temperature and strain rate ranges for which such denuded zones appear are different to those in Mg–23.5Ni alloy [27].

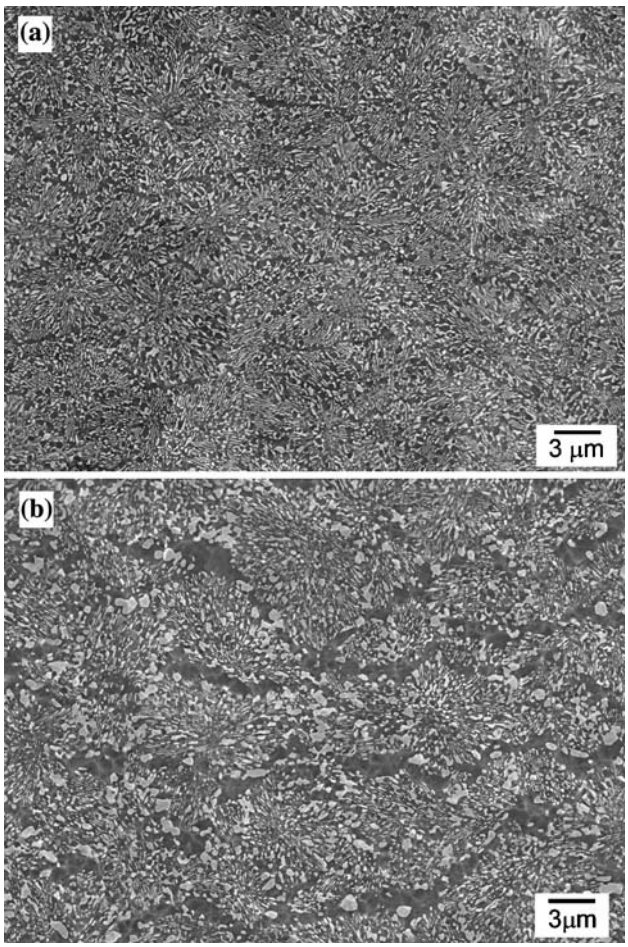

Fig. 4 Microstructures of ribbon annealed at 300 °C/90 min and tensile tested at: (**a**) 250 °C to 8% deformation and (**b**) 300 °C to 16% deformation

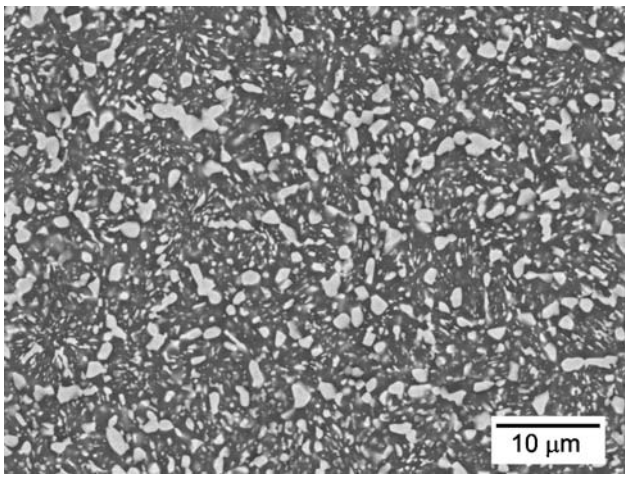

Fig. 5 Microstructure of annealed material at 400 °C/90 min after tensile test to strain of 13% at 300 °C

Discussion

The amorphous Mg–23.5Ni ribbons were obtained by melt-spinning technique and then subjected to annealing treatments at temperatures of 300 and 400 °C for 90 min to produce the crystallized materials. The annealing temperatures were selected above that corresponding to the crystallization of the Mg–23.5Ni amorphous alloy. Thus, a microstructure consisting of the phases predicted by the equilibrium diagram could be expected, namely Mg and Mg_2Ni phase. However, the morphology, size and distribution of both phases depend strongly on the annealing temperature, see Fig. 1, i.e. diffusion processes controlling the successive crystallization stages of amorphous Mg–23.5Ni.

Phase transformations occurring in the material during annealing at 300 °C for 90 min were described in Ref. [21]. The microstructure consists of Mg–Mg_2Ni eutectic domains embedding fine Mg grains. During the plastic flow, PFZs form at domain boundaries (Fig. 4). This suggests that domain size may play a relevant role in the mechanism controlling the deformation. It is appropriate,

therefore, to use the term "domain" or "domain size" instead of "grain" or "grain size" for microstructural description. In the case of ribbons annealed at 400 °C for 90 min, however, no rounded eutectic domains are formed, as shown in Fig. 1b. A well-formed structure consisting of Mg grains containing small Mg_2Ni particles is observed instead. This could explain why the grain size of the alloy treated at 400 °C is slightly smaller than the domain size of the alloy treated at 300 °C.

According to Fig. 2, it is concluded that both crystallized materials are brittle at room temperature, and their microhardness are higher than those generally reported for commercial Mg alloys. The large volume fraction of Mg_2Ni intermetallic particles could account for such brittleness. Also, it is often reported that the surface of ribbons obtained by melt-spinning is generally irregular, hence their thickness could be inhomogeneous. Consequently, stress concentration is expected to occur in some localized regions, which may cause premature failure of the ribbons, leading to low elongations to failure.

At temperatures below 150 °C both materials combine high strength and low ductility. In this case, it is assumed that soft Mg phase cannot support high work hardening in such a way that stresses, probably concentrated at the Mg/Mg_2Ni interface, cannot be released, promoting premature failure of the ribbons. As a first approach, this can be ascribed to the orientation relationship between the matrix and the Mg_2Ni interface. These assumptions can be supported by the fact that a marked influence of the orientation relationship between Mg and Mg_2Ni phases on the deformation modes and mechanical properties of eutectic Mg–Mg_2Ni alloys has been revealed [28]. Above 200 °C, however, such stress concentration is expected to decrease progressively with increase in the test temperature, so plastic deformation could proceed at low stresses.

The mechanical behaviour described above may be explained on the basis of the mechanisms controlling deformation at low and high temperatures. As illustrated in Fig. 3, the apparent stress exponent for both annealed materials is about $n_a = 4$ at strain rates close to 10^{-4} s^{-1} in the temperature range from 200 to 300 °C. In the literature, stress exponents of 4 (also 4.5 and 5) are generally associated with mechanisms involving slip (dislocations climb) [7, 11]. However, slip has been discarded as the mechanism controlling the deformation in the material annealed at 300 °C for 90 min at test temperatures above 300 °C [27]. In this case, a grain boundary sliding (GBS) mechanism is proposed to explain deformation behaviour and microstructural changes at such imposed test conditions.

In order to approach the deformation mechanism occurring in the crystallized materials in the temperature range up to 300 °C, strain rates are calculated according to the constitutive equations of the creep models given in Table 1. At a first sight, the slip pipe diffusion controlled mechanism and lattice and grain boundary diffusion controlled GBS mechanisms are not taken into account since they predicted stress exponent values of 7 and 2, respectively. Similarly, slip lattice diffusion controlled mechanism is discarded to explain the deformation behaviour of the Mg–23.5Ni alloy since the predicted strain rates diverge considerably from the experimental one, although the stress exponent of 4–5 is very close to the value determined in this study (see Table 1).

The GBS pipe diffusion controlled mechanism, however, shows an optimum concordance between predicted and imposed strain rate at test temperatures above 200 °C. Furthermore, the activation energies of 93 kJ/mol for annealed material at 300 °C and 115 kJ/mol for annealed material at 400 °C, are close to pipe diffusion in Mg. On the other hand, several microscopic TEM observations revealed strain fields at regions adjacent to the Mg/Mg_2Ni interphases, so it is reasonable to assume that they could act as sinks for dislocations during deformation. Therefore, these mechanical and structural features support that pipe diffusion controlled GBS should be the main mechanism controlling the deformation above 200 °C in both annealed materials.

Macroscopic examinations of ribbons annealed at 300 °C and deformed in tension above 200 °C show significant microstructural changes. Once the steady state is achieved in the true stress–true strain curves, PFZs are developed at domain boundaries at all test temperatures. They are located normal to the tensile axis and then they thicken slowly with straining progress. These relevant structural changes accompanying simultaneously the formation of the PFZs in deformed ribbons are depicted by microscopic observations. It is found that fine Mg grains move during deformation through the eutectic structure towards the domain boundaries. However, many Mg grains close to the core of the eutectic domains remain unaffected. These features manifest a clear evidence of occurrence of GBS process in the crystallized Mg–23.5Ni material [30, 31].

It is worth noticing that for the material annealed at 300 °C, the strain rate predicted by pipe diffusion controlled GBS mechanism is slightly lower than the imposed strain rate. This could probably be due to the fact that the domain structure does not facilitate easy GBS [27]. For the material annealed at 400 °C, the deformed microstructures above 200 °C resemble that of the non-deformed material (Fig. 5). These microstructures also indicate GBS operation.

It can be concluded, regarding the mechanical behaviour and the changes of the microstructure of the crystallized Mg–23.5Ni alloy during tensile test, that GBS pipe diffusion controlled should be the mechanism governing the deformation of this material at the strain rate of 10^{-4} s^{-1} at temperatures above 200 °C.

Table 1 Predicted strain rates according to the constitutive equations of different creep models. Experimental strain rate is 10^{-4} s^{-1} [26, 29]

Creep mechanism	Predicted strain rate (s^{-1}) Material annealed at 300 °C/90 min			Predicted strain rate (s^{-1}) Material annealed at 400 °C/90 min		
	200 °C	250 °C	300 °C	200 °C	250 °C	300 °C
Slip (lattice diffusion controlled), $n = 5$ $\dot{\varepsilon} = A_1\left(D_L/b^2\right)\left(\sigma/E\right)^5$	1.4×10^{-5}	9.2×10^{-6}	2.4×10^{-6}	9.5×10^{-6}	1.9×10^{-5}	1.3×10^{-5}
Slip (pipe diffusion controlled), $n = 7$ $\dot{\varepsilon} = A_2\left(D_p/b^2\right)\left(\sigma/E\right)^7$	1.9×10^{-4}	1×10^{-5}	2.3×10^{-7}	1×10^{-4}	2.8×10^{-5}	2.3×10^{-6}
Grain boundary sliding (lattice diffusion controlled), $n = 2$ $\dot{\varepsilon} = A_3\left(D_L/d^2\right)\left(\sigma/E\right)^2$	1.9×10^{-6}	1.2×10^{-5}	3.5×10^{-5}	3.11×10^{-6}	3×10^{-5}	1.3×10^{-4}
Grain boundary sliding (grain boundary diffusion controlled), $n = 2$ $\dot{\varepsilon} = A_4\left(D_{gb}b/d^3\right)\left(\sigma/E\right)^2$	5.3×10^{-3}	2.6×10^{-3}	6.5×10^{-4}	7.4×10^{-3}	8.7×10^{-3}	4.7×10^{-3}
Grain boundary sliding (pipe diffusion controlled), $n = 4$ $\dot{\varepsilon} = A_5\alpha\left(D_p/d^2\right)\left(\sigma/E\right)^4$	2×10^{-5}	4.3×10^{-5}	5.4×10^{-5}	4.5×10^{-5}	1.5×10^{-4}	2.8×10^{-4}

Values of constants A_1, A_2, A_3, A_4 and A_5 were taken from Ref. [31]. The Young's modulus, E, was calculated from the modified relationship for pure magnesium: E(MPa) $= 5.1 \times 10^4$ [1−5.3 × 10^{-4} (T-300)], $b = 3.21 \times 10^{-10}$ m, $\alpha = 4$, $k = 1.38 \times 10^{-23}$ J/K, $d = 12.4 \times 10^{-6}$ and 9×10^{-6} m for the material annealed at 300 and 400 °C, respectively (calculated as 1.776 × L, being L the linear intercept grain size), $D_L = 10^{-4}$ exp(-135000/RT) m^2/s, $D_{gb} = D_p = 7.79 \times 10^{-3}$ exp(−92000/RT) m^2/s

Conclusion

The following conclusions can be drawn:

1. Different microstructures were obtained after annealing the amorphous Mg–23.5Ni ribbons at 300 and 400 °C. After annealing at 300 °C the ribbon exhibited a lamellar structure, embedding Mg and Mg_2Ni. After annealing at 400 °C the lamellae structure was not observed. A well-defined microstructure consisting of Mg grains, outlined by coarse equiaxed Mg_2Ni particles, was instead observed.
2. Both annealed ribbons showed high strength and low ductility below 200 °C at strain rates close to 10^{-4} s^{-1}. This is related to the accumulation of stresses at the Mg/Mg_2Ni interface during the tensile test.
3. Above 200 °C particle free zones were formed during tensile test in annealed ribbons at 300 °C, but they were not observed in the material annealed at 400 °C. The deformation behaviour and the changes of the microstructure were explained in light of pipe diffusion controlled grain boundary sliding mechanism.

Acknowledgements M. Eddahbi thanks postdoctoral stage in *Departamento de Física—Universidad Carlos III Madrid*. The authors are grateful to MEC for financial support for this work under project MAT2003–02845.

References

1. Ridley N (1995) Superplasticity: 60 years after Pearson. The Institute of Materials, London
2. Bae DH, Kim SH, Kim DH, Kim WT (2002) Acta Mater 50:2343. doi:10.1016/S1359–6454(02)00067-8
3. Xu DK, Liu L, Xu YB, Han EH (2007) Mater Sci Eng A 443:248. doi:10.1016/j.msea.2006.08.037
4. Mohri T, Mabuchi M, Saito N, Nakamura M (1998) Mater Sci Eng A 257:287. doi:10.1016/S0921-5093(98)00853-3
5. Hara M, Morozumi S, Watanabe K (2006) J Alloys Compd 414:207. doi:10.1016/j.jallcom.2005.05.048
6. Spassov T, Rangelova V, Neykov N (2002) J Alloys Compd 334:219. doi:10.1016/S0925-8388(01)01745-5
7. Sherby OD, Burke PM (1968) Progr Mater Sci 13:1325. doi:10.1016/0079-6425(68)90024-8
8. Vagarali SS, Langdon TG (1982) Acta Metall 29:1969. doi:10.1016/0001-6160(81)90034-1
9. Vagarali SS, Langdon TG (1982) Acta Metall 30:1157. doi:10.1016/0001-6160(82)90009-8
10. Milička K, Čadek J, Ryš P (1970) Acta Metall 18:1071. doi:10.1016/0001-6160(70)90005-2
11. Poirier JP (1976) Plasticité à haute température des solides cristallins. Eyrolles, Paris, pp 291–297
12. Shi L, Northwood DO (1994) Acta Metall Mater 42:871. doi:10.1016/0956-7151(94)90282-8
13. Chung SW, Watanabe H, Kim W-J, Higashi K (2004) Mater Trans A 45:1266. doi:10.2320/matertrans.45.1266
14. Kim W-J, Chung SW, Chung CS, Kum D (2001) Acta Mater 49:3337. doi:10.1016/S1359-6454(01)00008-8
15. Watanabe H, Mukai T, Mabuchi M, Higashi K (2001) Acta Mater 49:2027. doi:10.1016/S1359-6454(01)00101-X
16. Inoue A (1998) Progr Mater Sci 43:365. doi:10.1016/S0079-6425(98)00005-X
17. Gleiter H (2000) Acta Mater 48:1. doi:10.1016/S1359-6454(99)00285-2
18. Mohamed FA, Li Y (2001) Mater Sci Eng A 298:1. doi:10.1016/S0928-4931(00)00190-9
19. Islamgaliev RK, Valiev RZ, Mishra RS, Mukherjee AK (2001) Mater Sci Eng A 304–306:206. doi:10.1016/S0921-5093(00)01440-4
20. Kempen ATW, Nitsche H, Sommer F, Mittemeijer EJ (2002) Metall Trans A 33:1041. doi:10.1007/s11661-002-0205-3
21. Pérez P, Garcés G, Adeva P (2004) J Alloys Compd 381:114. doi:10.1016/j.jallcom.2004.02.050
22. Inoue A, Ohtera K, Kita K, Masumoto T (1988) Jpn J Appl Phys 27:L1796. doi:10.1143/JJAP.27.L1796

23. Chen HS, Krause JT, Coleman E (1975) J Non-Cryst Solids 18:157. doi:10.1016/0022-3093(75)90018-6
24. Poirier JP (1976) Plasticité à haute température des solides cristallins. Eyrolles, Paris, pp 55–71
25. Jonas JJ, Sellars CM, McG Tegart WJ (1969) Metall Rev 14:1
26. Frost HJ, Ashby MF (1982) Deformation mechanisms maps "The plasticity and creep of metals and ceramics". Pergamon Press, Oxford, pp 44–45
27. Pérez P, Eddahbi M, Garcés G, Sommer F, Adeva P (2004) Scripta Mater 50:1039. doi:10.1016/j.scriptamat.2003.12.025
28. Eckelmeyer KH, Hertzberg RW (1972) Metall Trans 3:609. doi:10.1007/BF02642741
29. Kim WJ, Chung SW, Chung CS, Kum D (2001) Acta Mater 49:3337. doi:10.1016/S1359-6454(01)00008-8
30. Ke M, Hackney SA, Milligan WW, Aifantis E (1995) Nano Mater 5:689. doi:10.1016/0965-9773(95)00281-I
31. Hahn H, Padmanabhan KA (1997) Philos Mag 76:559. doi:10.1080/01418639708241122